SSRG International Journal of Civil Engineering
ISSN: 2348-8352/ https://doi.org/10.14445/23488352/IJCE-V13I3P119

Volume 13 Issue 3, 255-273, March 2026

Original Article

Explicit-Dynamics Assessment of Reinforced Concrete Frame Response under TNT Blast: Stand-Off, Charge Weight and Incidence Angle Effects

Basavaraj Gudadappanavar[1], M. Selvakumar[2], Mayura M Yeole[3], Vinayak A Hosur[4], Yuvaraja Dibdalli[5], Cesar Morales-Verdejo[6], Prashant Sunagar[7]

[1]*Department of Civil Engineering, SDM College of Engineering and Technology, Dharwad, Karnataka, India.*
[2]*Department of Civil Engineering, Rajalakshmi Engineering College, Chennai, Tamilnadu, India.*
[3]*Department of Civil Engineering, PCET's Pimpri Chinchwad College of Engineering and Research, Ravet, Pune, India.*
[4]*Department Civil Engineering, Dayananda Sagar Academy of Technology and Management, Bangalore, India.*
[5]*Centro Integrativo de Biología y Química Aplicada (CIBQA), Facultad de Ciencias de la Salud, Universidad Bernardo O'Higgins, General Gana, Santiago, Chile.*
[6]*Universidad Bernardo O´Higgins, Vicerrectoría Académica, Dirección General de Investigación, Innovación, Transferenciay Emprendimiento, General Gana, Santiago, Chile.*
[7]*Department of Civil Engineering, Sandip Institute of Technology and Research, Nashik, India.*

[5]*Corresponding Author : ydibdalli@uc.cl*

Received: 14 December 2025 Revised: 16 January 2026 Accepted: 21 February 2026 Published: 23 March 2026

Abstract *- The non-linear dynamic response of a Reinforced Concrete (RC) frame to external blast loading was examined in ANSYS Workbench Explicit Dynamics. A parametric matrix of 32 simulations was generated based on variations in equivalent charge weight (TNT) of 100, 200, 400, and 800 kg, stand-off distance 5, 10, 15, and 20 m, and angle of incidence 0° and 90°. The frame response was quantified using total frame deformation and equivalent von Mises stress and strain for both concrete and rebar. Frame response by deformation, stress, and strain was found to behave consistently with monotonic escalation for increased charge weight (range 100–800 kg) and strongly attenuated for increasing stand-off distance, 5 m to 20 m. Frame deformation was shown to be the most important parameter for mitigating blast loads, as increasing stand-off distance from 5 m to 20 m resulted in about a 79–92% reduction in peak deformation, depending on the charge weight and incidence angle. The angle of incidence also significantly influenced directional response demand and partitioning of the response; increasing the angle of incidence from 0° to 90° resulted in a 65% reduction of peak deformation in all simulations, with stand-off distance also being the most effective mitigation parameter. Reductions of equivalent strain were found to increase more than equivalent stress, with a 76% decrease in concrete and a 74% decrease in rebar. These findings enhance blast performance evaluation of concrete frames, identifying the effects of standard distances and loading direction on load-mitigation design.*

Keywords *- Blast loading, Explicit dynamics, Stand-off distance, TNT charge weight, Von Mises stress, Strain.*

1. Introduction

Unintentional explosion and intentional blast loading remain credible threats to civil structures, structural reinforced concrete (RC) buildings in particular, and extreme short-duration loading events. Unlike conventional loading, blast loading features peak overpressure and millisecond duration, resulting in inertia-dominated response, high-rate material response, and local-to-global failure propagation. The elastic design of conventional buildings to ultimate blast loading is uneconomical; blast-resistant design allows a controlled inelastic response, which permits significant deformation to reserve energy but avoids disproportionate collapse and the threat to life from debris.

Building blast loading depends on explosive yield, stand-off distance, detonation environment (external/internal, vented/confined), and angle of incidence, which define the pressure–time history of any surface exposed to blast loading. The positive phase of the pressure–time history is normally the most significant loading event, while the negative phase is less significant for member design.

The non-linear dynamic response of RC frames to blast loading, induced by cracking, spalling, reinforcement yielding, concrete crushing, and joint distress, motivates non-linear explicit Finite Element (FE) analysis to determine deformation and damage criteria under parametric variation.

Accordingly, this study subjects a representative critical RC frame to blast loading in ANSYS Workbench Explicit Dynamics under variation of TNT equivalent mass 100-800 kg, stand-off distance 5-20 m, and angle of incidence 0° and 90°. Structural response is defined in terms of peak total deformation and peak equivalent stress/strain in concrete and reinforcement, which provide a universal measure of response for performance assessment.

Despite extensive numerical and experimental research on reinforced concrete components under blast loading, the system-level response of RC frames subjected to external blasts remains insufficiently characterized, particularly with respect to the directional effects of blast incidence. Existing studies predominantly focus on charge weight and stand-off distance, while the influence of incidence angle on global deformation, strain accumulation, and damage mitigation has received limited systematic investigation. Furthermore, many frame-level studies rely on heterogeneous response indicators, limiting cross-comparison and design relevance. This study addresses these gaps through a solver-consistent explicit-dynamics parametric investigation of RC frame response under varying charge weight, stand-off distance, and incidence angle.

The novelty of this study lies in:

- systematic inclusion of blast incidence angle as a primary parametric variable at the frame level.
- use of solver-consistent global deformation and equivalent strain metrics to characterize performance across multiple blast scenarios.
- identification of stand-off distance and incidence angle as complementary mitigation mechanisms.
- development of a unified LS0–LS4 limit-state interpretation framework directly linked to explicit-dynamics solver outputs.

2. Literature Review

2.1. Conceptual Performance Chain for Blast Assessment

A mechanics-consistent conceptual framework for RC frame blast assessment is that of hazard, demand, damage, collapse, and consequence, allowing consistent interpretation between member- and system-level analyses. Hazard (H) is a function of charge weight, stand-off (scaled distance), detonation environment (internal/external), venting vs confinement, and the reflected/incident pressure field, usually estimated using Kingery–Bulmash/CONWEP-type relations or higher fidelity blast solvers. [3, 17] Demand (D) takes the form of pressure impulse time histories, member forces and rotations, peak/residual drift, energy absorbed, and is most reliably obtained through non-linear explicit dynamics for short-duration impulses. [1, 6, 10, 13] Damage (DM) appears as cracking, spalling/scabbing/perforation, yielding of reinforcement, and concrete crushing, and is usually represented using rate-sensitive material laws (e.g., RHT/JH/CDP families) along with erosion/deletion criteria such as IGS in explicit solvers. [9, 13, 17] Collapse (C) is due to local-to-global effects (column loss, joint degradation, redistribution) and is especially sensitive to the realism of boundary conditions and system connectivity. [4, 14, 16] Consequence (Q) includes considerations beyond collapse, such as residual capacity, repairability, downtime, and functional loss of secondary systems, which can outweigh performance issues even while the structure remains globally stable [6].

2.2. Numerical Modeling Paradigms for Blast Response

RC blast studies are dominated by non-linear explicit FEA in ANSYS AUTODYN/LS-DYNA, Abaqus/Explicit, and increasingly ANSYS Workbench Explicit Dynamics. [1, 3, 4, 6, 8, 13, 17] Two consistent elements are: (i) blast loading is determined using scaled-distance concepts, Kingery–Bulmash/CONWEP pressure–time histories, and JWL equations of state when detonation products are modeled explicitly; [3, 17] and (ii) rate-sensitive material/damage modeling, with concrete represented using RHT/Johnson–Holmquist/CDP-type laws and reinforcement using elasto-plastic laws often Johnson–Cook to account for the beneficial effects of high-rate loading on strength and damage evolution [3, 8, 11, 12, 13, 17].

A practical distinction exists between unified blast–air–structure simulations (AUTODYN/LS-DYNA) and purely structural explicit dynamics Ansys workbench that utilize imported pressure–time histories. [1, 6, 9, 10, 13, 17]. This has practical importance in modeling the effects of internal or partly vented blasts, where the interaction effects, reflections, venting, etc., may not be adequately captured by a simplified approach to loading. [14, 18]

2.3. ANSYS-based Explicit Workflows and Validation

In ANSYS/LS-DYNA workflows, concrete is modeled with 3D solids, reinforcement with beam/embedded approaches, and fluid structure interaction (FSI) is included when air/TNT is explicitly modeled. [1, 9, 13, 17] Spalling/perforation is implemented via erosion/deletion criteria (e.g., IGS), which introduces calibration sensitivity and model-form uncertainty. [9, 17] Workbench Explicit Dynamics is used preferentially where the response of the structure, rather than the blast-wave propagation, is of concern, loading through pressure time histories using empirical relations or code-based models.

[6, 10] Validation practice is variable; some studies calibrate to component/full-scale blast tests for peak displacements, cracking, and damage patterns, which enhances validity; [9, 13, 16] others rely mainly on literature calibration or code-type criteria, introducing potential for high uncertainty especially when loads differ significantly between modeling strategies [3, 6, 10, 12, 17].

2.4. Response Characterization: Local Damage, System-Level Deformation, and Collapse Evolution

Three interrelated themes dominate: (i) member damage response at the column/beam/slab-level focusing on damage indices, failure-mode transition and residual capacity; [2, 5, 9, 11, 13, 15] (ii) frame response and progressive collapse at the 3D frame level for external/internal explosions; [1, 3, 4, 10, 14, 16] and (iii) parametric detailing level fragility curves/retrofit detailing, concrete grade, infills, connections/retrofit techniques. [1, 4, 9, 12, 15] Failure-mode transition is a common synthesis topic: close-in blasts generally favor punching/shear-type local failure modes while a larger scaled distance and better detailing promote a flexural response; transverse reinforcement, axial load ratio, and concrete grade influence this transition. [1, 2, 11, 13, 15] However, damage criteria (plastic strain limits, damage indices, rotation limits) differ widely between studies, complicating comparability and generalization to design requirements [2, 13].

2.5. Evidence Clustering Frame Studies vs Component Studies

Frame/substructure studies primarily address global robustness/collapse modes. Abebe and Mohammed emphasize the authenticity of 3D modelling and boundary conditions for joint behaviour and load transfer. [1] Xu et al. evidence that masonry infill limits the collapse probability in column loss cases. [4] Jiang et al. propose empirical M–R curves for substructure close-in blast damage. Li et al. for orthogonal design rank blast parameters in frame building. [14] Full-building Abaqus/Explicit models are method-comparators for building/system-level response. [3, 16] Component studies generate more generalizable quantitative relations for calibration.

Li et al. derive a damage coefficient–scaled distance relation for RC columns, [2] Shen et al. max rotation relations empirical for function of eccentricity, blast position, reinforcing ratio, axial load, blast to beams field tests that couple fluid–structure models. [8] Other studies inform prestressed beams, slab damage under TNT, DIC validated columns' response, concrete grade, and ratio impact. [11, 13, 15] Cross-cutting studies identify that blast-load representation may dominate uncertainty: Polyakov and Lapenko's huge variation between analytical, Kingery–Bulmash, and AUTODYN results directly impacts pressure–time histories for solver; [17] erosion/IGS calibration can similarly shift local damage. [9]

2.6. Research Gap

The literature review identifies six unresolved gaps that trigger an ANSYS AUTODYN Workbench explicit workflow.

A careful review of the literature reveals unresolved methodological and conceptual limitations that undermine the reliability, transferability, and resilience implications of existing blast-response analysis of reinforced concrete frame systems.

Most studies concentrate on isolated components or idealized frame concepts, neglecting the inherently 3D nature of load transfer, joint interaction, and boundary-condition effects that characterize system-level response.

The inability of standard explicit dynamic analyses performed directly in structural solvers to capture interaction-driven pressure evolution means that pressure–time histories must be generated in a physically consistent manner in a hydrodynamic blast environment and imported into a structural solver to allow proper full-frame response evaluation, response envelope extraction, collapse characterization, and solver-sensitivity evaluation.

Most studies remain case-specific in the response information they provide. They offer limited value for use in practice or in future performance predictions. Without calibration against component-level behavior and moment–rotation relations, the findings of these studies cannot be used in a parametric manner. Literature lacks a parametric modeling approach capable of constructing response surfaces, identifying the ranking of governing parameters, and extracting simplified, robust performance measures.

Systematic omission of non-structural and secondary systems remains a major limitation. While infill panels account for much of the global stiffness, load redistribution, and damage progression within a concrete frame structure, they are usually ignored or idealized. The lack of interface modeling means their influence on drift demand and robustness may not be conservatively estimated.

Uncertainty related to blast load representation and material models is not routinely addressed. Empirical blast loads and physics-based hydrodynamic simulations are not compared in a normalized framework, and structural responses are not made to the sensitivity to erosion criteria and constitutive parameter settings. The contribution of load modeling inaccuracies and material idealizations to prediction uncertainty remains unquantified.

The lack of a canonical damage interpretation framework still hampers the comparison of damage findings across studies. Different damage indicators and failure definitions remain in use across studies, leading to findings that are sometimes incompatible or conflicting.

A unified scheme for classifying damage and collapse that ties directly to the variables used in solvers to determine damage and that validates these damage classifications against benchmarked behavior of analyzed components is needed for an objective view of damage from blast loading.

Most studies emphasize peak response over residual capacity, which is at the heart of resilience-based assessment. The dimensions of post-blast stiffness degradation, residual drift capacity, and damage reparability have received little attention. There have been no procedures for follow-on loading to assess post-event performance. Resilience-based assessment remains unaddressed in existing studies.

Explicit-dynamics modeling of Reinforced Concrete (RC) frame response to TNT blast loading is a crucial method of limiting explosive damage to structural frames. Previous research consistently finds that dynamic response and damage to RC systems are dependent upon the fundamental characteristics of the applied blast load, including stand-off distance, charge weight, and angle of incidence of the blast wave. Such parametric variation alters the magnitude of the pressure and impulse imparted to the affected frame due to the blast wave, as well as its non-linear response to the loading.

The numerical modeling of RC structures is a common application of contemporary finite element methods, including explicit-dynamics solvers such as Abaqus/Explicit and LS-DYNA. In these studies, elements typically utilize both Concrete Damaged Plasticity (CDP) and strain-rate dependent material models to capture the damage processes of cracking, spalling, and crushing, as well as the yielding of the reinforcement members.

Models of RC slabs subjected to air-blast pressures from TNT explosives at varying stand-off distances have revealed that the material and geometric cover parameters, the ratio of reinforcement to concrete area, and the compressive strength of the concrete itself significantly influence the deformation demand and extent of damage suffered (Ahmadi et al., 2021). Such findings illustrate the importance of such frame construction details in the accurate modeling of even explosive blast loads.

Among the key characteristics of a blast load, the angle of the stand-off distance has been shown to be the most significant governing parameter. As the distance increases between the explosive source of the blast wave, the explosive itself, and the frame, its damaging effects are significantly dampened due to wave attenuation. In relation to explicitly modeled RC frames, numerical models of RC columns subjected to blast loading conditions at close stand-off distances have revealed that smaller scaled distances lead to combinations of pressure and impulse that result in extremely damaging local conditions and a large loss of capacity in the remaining post-blast structures (Abedini et al., 2020). Thus, these relatively simple, quantified parameters have been established as indicators of the blast loading intensity that will be experienced by the affected frame. This characteristic of stand-off distance is reflected in many extant standards for blast-resistant design, where this single parameter is used as the controlling variable limiting exposure.

Charge weight is another measurable variable affecting the characteristics of blast loading. Charge weight represents a variable known that directly controls the energy output of an explosive blast. This energy output is significant in relation to the severity of the blast wave produced. Numerical modeling studies of TNT blast loads on RC slabs demonstrate that increased charge weight causes relatively predictable changes in the demand experienced by those frames.

Increased weight leads to increased peak pressures and impulses, which in turn result in increased deformation demands. These conclusions reflect consistent patterns among different parametric numerical models of RC slabs (Tiwari et al., 2017; Dua and Braimah, 2020). In addition, studies have established empirical equations to calculate the “critical” weights of TNT necessary to damage or destroy different sizes and types of RC frames using their reinforcement ratios and areas as variables (Silva and Lu, 2009; Dua and Braimah, 2020). Collectively, these studies help provide a framework for charge weight as a primary control variable for blast-resistant design.

In contrast to charge weight, incidence angle is an input that has not been as widely studied. Relatively little quantifiable research has been published regarding its effects on RC frames specifically. However, available studies have documented the effects of the incidence angle of other structural systems, indicating that it produces different deformation patterns and damage distributions within those structures (Tiwari et al., 2017). This difference occurs because the incidence angle alters the projection of pressure and impulse transfer dynamics of the blast wave within those affected structures. Thus, by explicitly including incidence angle as an additional variable in explicit-dynamics modeling, researchers can more realistically recreate blast-loading conditions in numerical experiments.

Explicit-dynamics modeling also enables recognition of additional factors that may be important controls on the type and extent of blast damage to RC frames. Several previous studies recognize local damage processes like concrete erosion, spalling, and fracture as significant factors in a variety of blast events. To appropriately account for those somewhat unpredictable processes, often difficult to quantify in uniform modeling studies, techniques such as erosion criteria are calibrated to specific experimental case outcomes.

In these cases, loss of elements that occur due to local damage can be applied to model the effects of local damage on the performance of the remaining components while maintaining stability in the experimental model (Luccioni et al., 2013). Reinforcement detailing also noticeably affects the amount and location of damage within affected structures. Reinforcement ratios (as well as spacing) for even longitudinal reinforcements also affect the remaining energy absorption capacity within those systems during modeling experiments (Ahmadi et al., 2021; Dua and Braimah).

In sum, these studies indicate that explicit-dynamics modeling can effectively be used to simulate frame responses to blast loads. They also show that two specific parameters of the blast load can be interpreted as significant or controlling variables: stand-off distance and charge weight. Finally, by incorporating that information into an additional parametric control for an experimental design variable, effective model-based retrofitting or design methods for RC frames can be developed to limit their susceptibility to damaging projectile threats.

2.7. Objectives of the Study

This study aims to evaluate and characterize the non-linear transient response of a prototypical Reinforced-Concrete (RC) frame to external TNT blast loading in ANSYS Workbench Explicit Dynamics, with the following goals:

By completely simulating its blast response for a parametric study of TNT-equivalent charge mass (100–800 kg), stand-off distance (5–20 m), and incidence angle (0° and 90°) over an extensive range to evaluate its inertia-dominated response to impulsive loading

By obtaining physically meaningful peak-response quantities from the explicit time-history solution, such as the maximum global deformation demand and equivalent (von Mises) stress/strain demand in the concrete and reinforcement, to provide a uniform performance metric to compare the response to various blasts

By applying that deformation and equivalent stress/strain demand as solver-consistent response metrics to provide a consistent basis for comparing the performance response to various blast load severity, direction, and stand-off distance as a potential mitigation measure.

2.8. Methodology Adopted

A coupled hazard-to-demand-to-response workflow is used, with code-consistent blast parameters first converted to face-specific pressure–time histories and then imposed on an explicit 3D RC frame in ANSYS Workbench to resolve the short-duration non-linear transient response. The hazard is specified according to cube-root scaling per IS 4991:1968, with charge weight and stand-off distance used to calculate scaled distance and scaled time, which are both mapped to peak pressure and duration descriptors.

2.8.1. Blast-Load Definition and Pressure–Time History Synthesis

Blast loading is specified through cube-root scaling, with scaled distance defined with respect to stand-off distance and TNT-equivalent yield, and scaled time employed to recover absolute phase durations; peak incident overpressure is also validated in IS 4991:1968 compliant ways by checking against standard correlations (e.g., Newmark, Mills, Kinney–Graham).

For each blast case, face-specific pressure histories are synthesized by: (i) specifying charge weight, stand-off distance and geometry of the target building and exposed face; (ii) calculating scaled distance according to IS 4991; (iii) retrieving peak incident pressure, reflected pressure, dynamic pressure, positive-phase duration, and triangular equivalent duration using IS-compliant validated pressure correlations; (iv) converting scaled-duration values back to absolute time; and (v) imposing the pressure–time function to the exposed face(s) for explicit analysis.

2.8.2. Explicit Dynamic FE Modeling in ANSYS Workbench

An (identically-sized) representative “critical” RC frame is reconstructed in ANSYS Workbench Design Modeler; concrete is modeled as 3D solids, and reinforcement as idealized embedded line/beam representations consistent with explicit time-integration assumptions and realistic rebar–concrete interdependency.

The domain is explicitly meshed (using HEX-dominant mesh suitable for stable explicit integration); interaction between steel and concrete is modeled through the Workbench embedded reinforcement coupling option; all other body interactions are set to frictionless to avoid numerical issues under extreme high-rate loading; conservative restraint is applied along the bottom of the frame through a fully-fixed support condition; analyses are performed using the Explicit Dynamics (AUTODYN) solver over a 0.01 s time span to capture the dominant positive-phase loading driven response demands.

2.8.3. Parametric Matrix and Output Extraction

A structured parametric matrix is sampled over stand-off distance, charge weight, and incidence angle, resulting in a 32-case explicit simulation matrix.

For each case in the matrix, peak response demands are read out from the explicit time histories as max total deformation, von Mises stress (and strain) in concrete and reinforcing steel, enabling consistent comparison of response demand severity and partitioning between cases.

Integrated Explicit-Dynamics Workflow for Blast Assessment of Reinforced Concrete Frame Structures is given below in Plate 1.

3. Blast-Load Definition and Implementation in Ansys Workbench

This study completes the hazard demand link by (i) defining and parameterizing blast strength using IS:4991-1968 scaling, and conventional overpressure relationships, and (ii) implementing the pressure–time load histories in ANSYS Workbench Explicit Dynamics to record the RC frame’s transient deformation and stress/strain response.

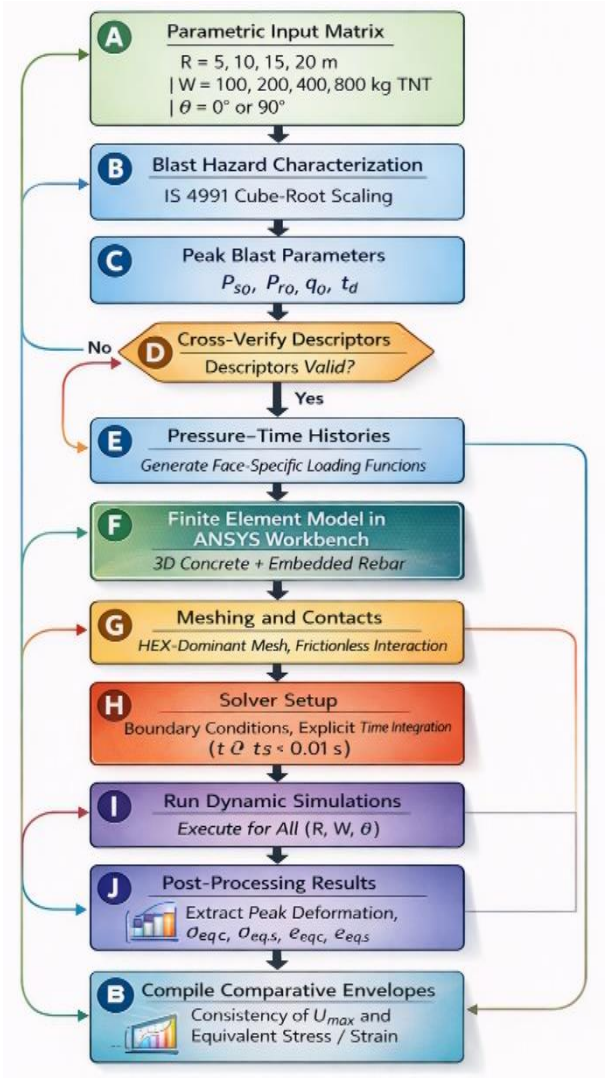

Fig. 1 Methodology adopted in the present study

3.1. Design Blast-Load Definition

Before a blast load could be predicted, the theoretical structure size needed to be established. This was for theoretical purposes only and did not play a significant role in our analysis. Figure 2 shows the width and length of the structure. Design blast load refers to a blast load that has a reasonable probability of occurrence in and around the structure, and for analytical investigation, it is described in the form of a plot between pressure and time for a specified charge weight and stand-off distance.

Most severe blast loading on any face of a structure is produced when the structure is oriented with the face normal to the direction of propagation of the shock front. However, for lack of known orientation of future explosion, every face of the structure shall be considered as a front face. When the blast field surrounds the structure, the difference in pressures on the front and rear faces tends to tilt and overturn the structure.

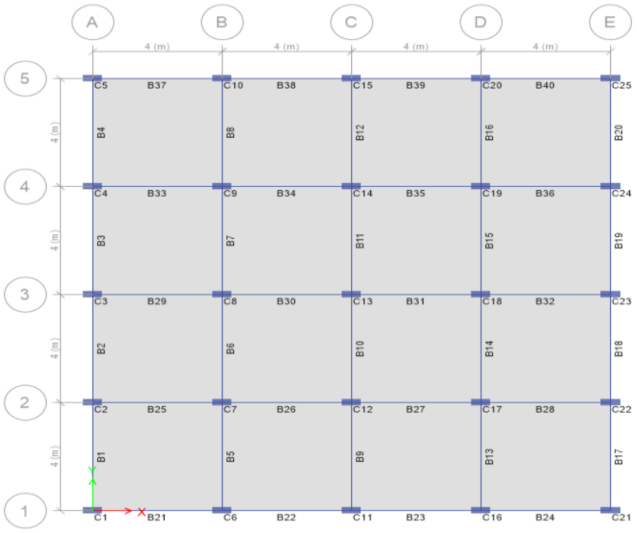

Fig. 2 Building layout for blast calculations

3.2. Scaling Law

All blast parameters are primarily dependent on the energy released by detonation in the form of a blast wave and on the distance from the explosion. Scaling laws provide parametric correlations between a particular explosion and a standard charge of the same substance. The scaling law used as specified by IS: 4991-1968 is given as follows. Equations 1 to 6 gives the details of the same.

Blast effects are parameterized using cube-root scaling:

$$x = \frac{R}{W^{1/3}}, \qquad t_0 = \frac{t}{W^{1/3}} \tag{1}$$

Where W is TNT-equivalent yield (tonnes), R is stand-off distance, x is scaled distance used to obtain peak/duration parameters Table 1, and t_0 is the corresponding scaled time.

3.3. Peak Incident Overpressure Correlations

Peak incident overpressure P_{so} is estimated as a function of scaled distance (notation interchangeable with x depending on source) using standard relations for cross-validation:

$$P_{so} = \frac{6.7}{Z^3} + 1 \text{ bar} \quad (P_{so} > 10 \text{ bar}) \tag{2}$$

$$P_{so} = \frac{0.975}{Z} + \frac{1.455}{Z^2} + \frac{5.85}{Z^3} - 0.019 \text{ bar} \quad (0.1 < P_{so} < 10 \text{ bar}) \tag{3}$$

Newmark

$$P_{so} = 6784\left(\frac{W}{R^3}\right) + 93\left(\frac{W}{R^3}\right)^{1/2} \tag{4}$$

Mills (kPa)

$$P_{so} = \frac{1772}{Z^3} + \frac{114}{Z^2} + \frac{108}{Z} \tag{5}$$

Kinney–Graham (bar)

$$P_{so} = \frac{808\left[1+\left(\frac{Z}{4.5}\right)^2\right]}{\sqrt{\left[1+\left(\frac{Z}{0.048}\right)^2\right]}\sqrt{\left[1+\left(\frac{Z}{0.32}\right)^2\right]}\sqrt{\left[1+\left(\frac{Z}{1.35}\right)^2\right]}} \quad (6)$$

3.4. Pressure-Time History Generation

Face-specific pressure histories are generated as follows: Defining W, R, and building dimensions (Figure 2). Compute scaled distance x (IS:4991-1968). From IS 4991:1968 "Criteria for Blast Resistant Design of Structures for Explosions Above Ground" (Table 1, Clause 5.1) validated correlations, obtain: Pso, reflected overpressure Pro, dynamic pressure q_0, positive phase duration t_0, and equivalent triangular duration t_d.

Convert scaled durations to absolute values using $W^{(1/3)}$ where applicable. Compute face pressures considering clearance time, t_d, drag effects, and geometry-dependent exposure. Apply pressure–time functions to the relevant faces for analysis.

Pressure-time histories for 100, 200, 400, and 800 kg TNT are derived for the above stand-off distances and incidence cases.

3.5. Explicit Simulation in ANSYS Workbench

The explicit solver in ANSYS Workbench is used to evaluate the short-duration non-linear response under the pressure-time loads derived, and obtain peak deformation, equivalent stress, and equivalent strain for comparison for R, W, and incidence.

3.5.1. Notes on Equations of State (EOS)

EOS definitions are required when the blast wave is explicitly modelled, an AUTODYN-type model with TNT. For interest, standard forms of EOS equations are noted as shown in Equations 7 to 10:

JWL EOS

$$p = A\left(1-\frac{\omega}{VR_1}\right)e^{-VR_1} + B\left(1-\frac{\omega}{VR_2}\right)e^{-VR_2} + \frac{\omega e_0}{V}, \qquad V = \frac{\rho_e}{\rho} \quad (7)$$

P–α EOS (porosity/compaction)

$$\alpha = \frac{v}{V_{solid}} = \frac{\rho_{solid}}{\rho} \quad (8)$$

Polynomial EOS (matrix material)

$$p = A_1\mu + A_2\mu^2 + A_3\mu^3 + B_0 + B_1\mu\rho_0 e \quad (\mu \geq 0) \quad (9)$$

$$p = T_1\mu + T_2\mu^2 + B_0\rho_0 e \quad (\mu < 0), \qquad \mu = \frac{\rho}{\rho_0} - 1 \quad (10)$$

4. Finite Element Model and Analysis Setup

This chapter covers the modelling aspects of the analysis of frame response to the defined blast loading: material models, geometry, reinforcement, idealization, discretization/contact assumptions, boundary conditions, solver settings, and parametric matrix analysis.

4.1. Material Models

Materials are defined for non-linear transient response to blast loading. TNT, reinforcement steel (bilinear isotropic hardening), and concrete (CONC-35MPA set) are employed; complete parameter definitions are in Tables 1, 2, and 3, and the steel hardening curve is shown in Figure 3.

Table 1. Properties of TNT

Property	Value
Material	TNT
Density	1630 kg/m³
JWL parameter A	3.7377 × 105 MPa
JWL parameter B	3.7471 × 103 MPa
JWL parameter R1	4.15
JWL parameter R2	0.90
JWL parameter ω	0.35
Detonation velocity	6930 m/s
Energy per unit mass	3.681 x 106 J/kg
Chapman-Jouguet pressure	2.10 × 104 MPa

Table 2. Properties of Structural Steel

Property	Value
Material	Structural Steel NL
Density	7830kg / (m^3)
Young's modulus, E	2.00 ×10^{11} Pa
Poisson's ratio, v	0.30
Bulk modulus, K	1.67×10^{11} Pa
Shear modulus, G	7.69×10^{10} Pa
Yield strength	4.15×10^8 Pa

Table 3. Material Properties of Concrete

Property	Value
Material	CONC-35 MPa
Density	2314kg /m3
Compressive strength	35 MPa
Bulk modulus (K)	3.527 × 10^{10} Pa
Shear modulus (G)	1.67 × 10^{10} Pa
Parameter A1	3.527 × 10^{10} Pa
Parameter A2	3.958 × 10^{10} Pa
Parameter A3	9.04 × 10^{10} Pa
Parameter B0	1.22
Parameter B1	1.22
Parameter T1	3.527 × 10^{10} Pa
Parameter T2	0
Solid density	2750kg / (m^3)
Porous sound speed	2920 m/s
Initial compaction pressure	2.33 × 10^7 Pa
Solid compaction pressure	6 × 10^9 Pa
Compaction exponent	3

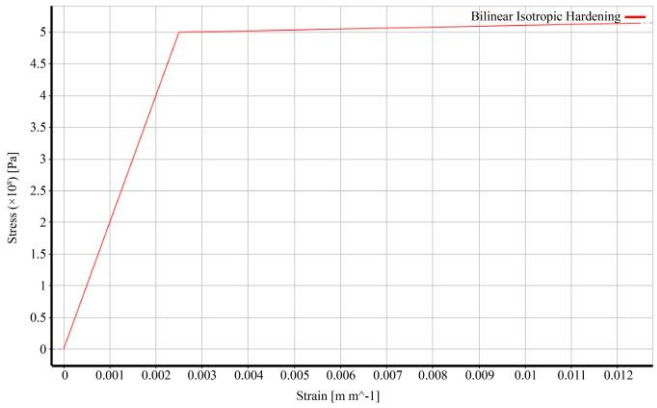

Fig. 3 Stress strain curve-bilinear isotropic hardening

4.2. Geometry Idealization

The critical RC frame (from ETABS) is modelled in Ansys Workbench Design Modeler. Concrete is modelled with solid 3D geometry; reinforcement is idealized as line/beam (embedded) elements shown in Figures 4 and 5. The geometry of the explosive source is modelled as per the selected charge cases.

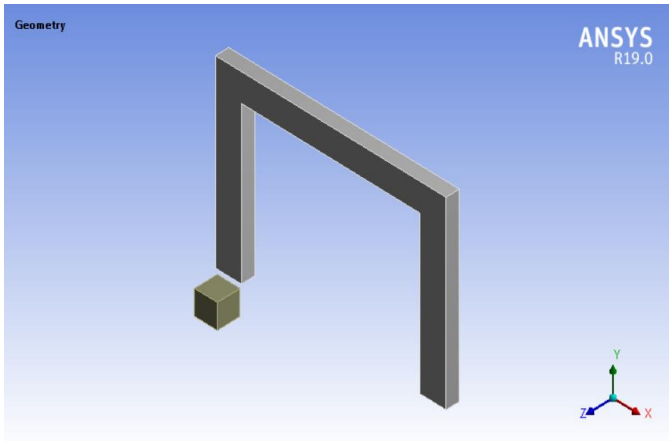

Fig. 4 Geometry-RC frame

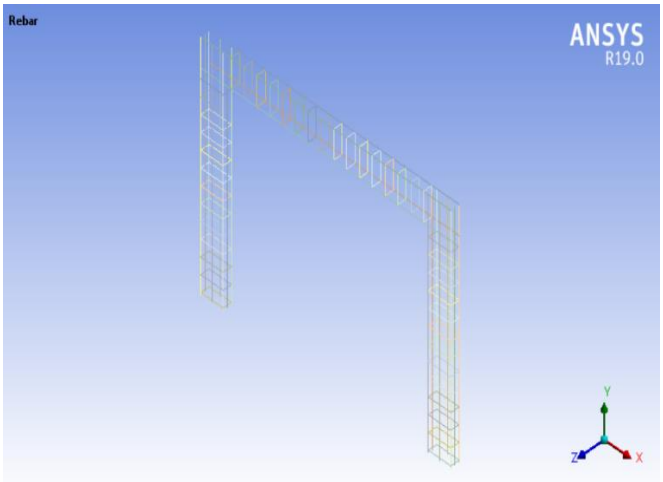

Fig. 5 Geometry- Rebar

4.3. Discretization and Interactions

The model is discretized with HEX-dominant elements that allow stable explicit integration, shown in Figures 6 and 7. Concrete–rebar interaction is defined using the coupling option of the reinforcement; contact and body interaction is set to frictionless to prevent numerical instability issues under rapid loading.

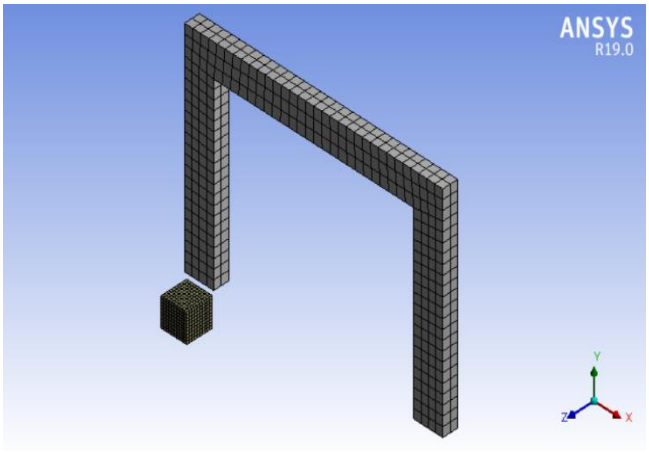

Fig. 6 Meshing of Geometry

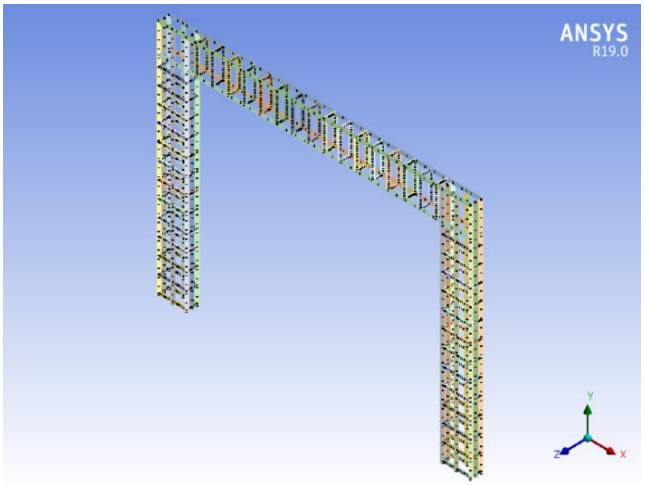

Fig. 7 Meshing of Rebar

4.4. Boundary Conditions and Solver Controls

The base of the frame is fixed to provide conservative support conditions. Analyses are performed in Explicit Dynamics with the AUTODYN solver, with a chosen analysis end time of 0.01 s to capture the essential positive-phase-driven response and demands.

4.5. Parametric Matrix

A structured study is conducted over stand-off distance, charge weight, and incidence angle, as shown in Table 4.

R = 5, 10, 15, 20 m
W = 100, 200, 400, 800 kg TNT
Incidence angles = 0° and 90° are shown in Figures 8 and 9.

Table 4. Parameters used for analysis

Stand-off Distance	5m	10m	15m	20m
Charge Weight	100kg	200kg	400kg	800kg
Angle of Incidence	0˚	0˚	90˚	90˚

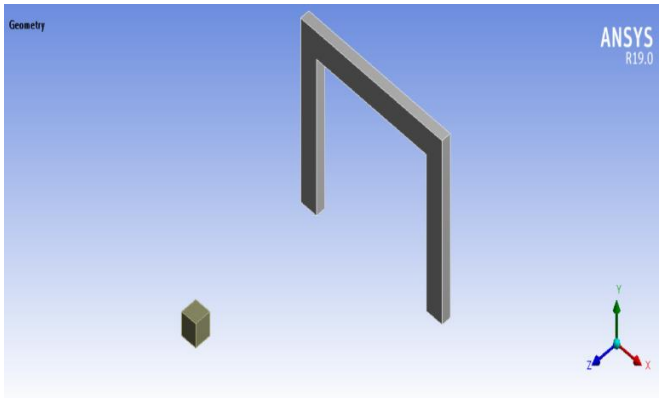

Fig. 8 Angle of Incidence 0˚

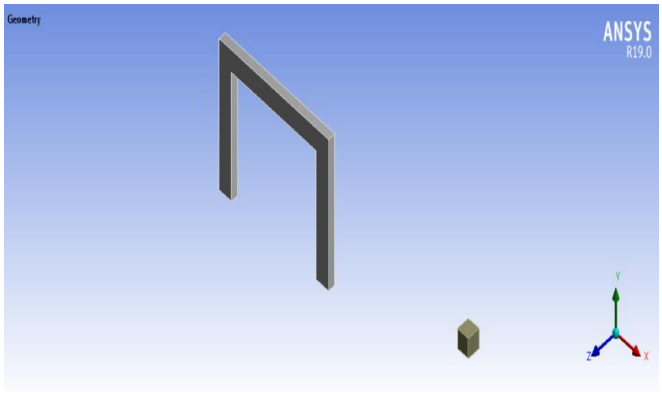

Fig. 9 Angle of Incidence 90˚

Non-linear explicit-dynamic simulations have been performed to determine the transient blast response of a prototypical RC frame to TNT-equivalent detonation loading, with a structured 32-case parametric matrix of stand-offs R=5, 10, 15, and 20 m, charge weights W=100, 200, 400, and 800 kg, and two incidence angles θ=0∘ and 90∘. The short-duration explicit time histories were post-processed to compute peak response demands, including maximum global deformation Umax and equivalent stress and strain in concrete ($\sigma_{eq,c}, \varepsilon_{eq,c}$), and equivalent stress and strain in reinforcement ($\sigma_{eq,s}, \varepsilon_{eq,s}$).

The results indicate monotonic demand increases with charge weight and significant attenuation with stand-off distance. The increasing stand-off distance from 5 m to 20 m results in a 79–92% reduction in U_{max} for the entire parametric matrix. For the most demanding loading case (W=800 kg), this is a drop from 1601.4 mm to 306.08 mm (80.89% reduction) at θ = 0°, and from 529.38 mm to 81.108 mm (84.68% reduction) at θ = 90°, confirming stand-off distance as the dominant geometric mitigation parameter. Incidence angle (θ) exhibits a similarly strong effect on deformation-controlled response demands. Normal incidence compared to oblique incidence shows mean reductions of 65.16% in deformation, 76.36% in concrete equivalent strain, and 74.18% in reinforcement equivalent strain, with stress reductions being more pronounced for steel than for concrete. These results suggest that incidence angle primarily mitigates deformation-induced damage effects, and flexural effects and localized effects of strain are expected to be the dominant failure mechanism in the absence of such mitigation.

To ensure performance-based evaluation of the results is presented in a consistent fashion, a LS0–LS4 limit-state classification scheme is proposed, which accommodates the model solver outputs and relates deformation and strain demands to damage levels expected as a function of the severity of damage and the typical time progression of damage severity associated therewith. This provides a basis for comparison in assessing the performance-based effects of blast loading on structures with respect to various parameter combinations with respect to charge weight, stand-off distance, and orientation.

4.6. Model Validation and Benchmarking

No direct experimental validation was performed in the current study due to its parametric, system-level response profiling of RC frames to blast loading. Validation is achieved through benchmark comparison with literature studies, however.

The blast loading model, material modeling strategy, and the observed response behavior (e.g., the monotonic behavior of deformation and strain with charge weight, and the pronounced attenuation of response with stand-off distance) are consistent with those that have been experimentally validated for RC slabs, columns, and frames subjected to external blast loading.

RC response behavior has been established in earlier studies, and particularly those that were validated against field or laboratory blast tests using explicit-dynamics solvers. This includes the deformation-dominated response in the close-in regions and the mitigating effect of scaled distance on the damage severity. The consistency of the current study with these established trends supports the use of the predictions of system-level behavior in the current numerical study. The aim of the validation process is trend fidelity and physical realism, not providing an exact quantification of a single, specific experimental scenario.

4.7. Material Model Justification

The chosen material constitutive models ensure physical realism, numerical robustness, and computational efficiency in simulating the behavior of materials subjected to high-strain-rate loading conditions. Concrete was modeled using a non-linear damage formulation, which is able to represent cracking, crushing, stiffness degradation, and irreversible response in the context of blast loading.

While models such as the RHT or Johnson–Holmquist models exist, those that were used in the current study offer a stable, well-understood method of representing concrete behavior at the system level, where global deformations and strains are the main focus of the analysis.

Reinforcement steel was represented using an elastoplastic constitutive model with isotropic hardening, which is sufficiently accurate in modeling yielding and post-yield behavior for reinforcements subjected to loading rates typical of blast scenarios.

The use of embedded reinforcement elements enables stable load transfer between concrete and steel without the artefacts associated with contact-based reinforcement assignments. This approach has been justified by its use in a multitude of published simulations of blast-response studies, which have been established to reproduce realistic stress–strain demands for reinforcements subjected to impulsive loading.

4.8. Mesh Sensitivity and Numerical Stability

Mesh discretization was performed to ensure that the explicit time-integration solver was stable, while keeping computational costs manageable. A structured HEX-dominant mesh was employed for the concrete domain, which permits good aspect ratios for individual elements, while minimizing hourglass and distortion effects under the influence of large, induced deformations. Reinforcement elements were discretized to be compatible with the surrounding concrete elements.

The mesh density was refined until further refinement produced no significant difference in response values of interest, such as maximum global deformations and peak equivalent strains for concrete and reinforcements. This qualitative approach to assessing mesh sensitivity ensures that the reported results are not artifacts of mesh discretization. Further, stable time stepping by the explicit solver was ensured using the smallest element dimensions and material wave speeds to ensure numerical stability during all phases of the simulation.

4.9. Blast Load Representation

Blast loading was implemented according to empirically validated pressure–time histories, which are standard for cube-root scaling relations. The blast scenario's geometrical parameters of stand-off distance and TNT-equivalent charge weight served as surrogates for establishing peak overpressures and positive-phase durations. These were applied as time-varying pressures to the blast-exposed surfaces of the structure. This modeling level is appropriate for external air-blast scenarios, where the focus is on structural response rather than fine-scale effects of the blast-wave propagation.

The methodology used for blast-load representation follows common modeling steps, such as those that were employed in the published simulation models on which the current one was based. The approach has been utilized in a number of numerical studies, which have themselves been verified against real experimental blast test data.

Effects of fluid–structure interaction are not modeled in this instance; however, imposed pressure–time histories are expected to dominate the impulse imparted to structures by external air blast scenarios that produce their deformation in response to the specific scenarios examined.

5. Results and Discussion

5.1. Peak-Response

Explicit dynamic simulations were performed for a total of 32 blast scenarios across the stand-off distances m, TNT-equivalent charge weights W= 100, 200, 400, 800 kg, and incidence angles zero and 90 degree For each of the simulations, peak response quantities were harvested from the explicit time histories for two distinct structural domains: (i) the reinforced-concrete frame, as inferred from maximum global deformation U_{max} and concrete equivalent stress and strain ($\sigma_{eq,c}, \varepsilon_{eq,c}$); and (ii) the reinforcement, represented by equivalent stress and strain ($\sigma_{eq,s}, \varepsilon_{eq,s}$). Local contour plots are presented in Figures 10–14 to convey a representative spatial distribution of damage and demand, while parametric response envelopes and comparative plots for the entire simulation matrix are presented in Figures 15–24.

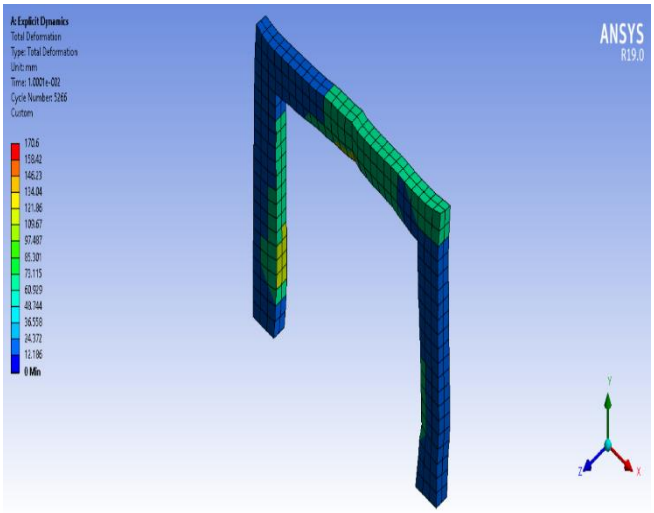

Fig. 10 Total deformation for 5m, 100kg

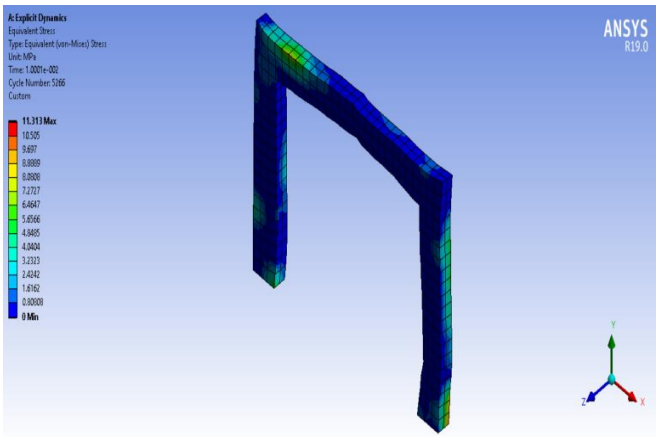

Fig. 11 Equivalent stress for 5m, 100kg

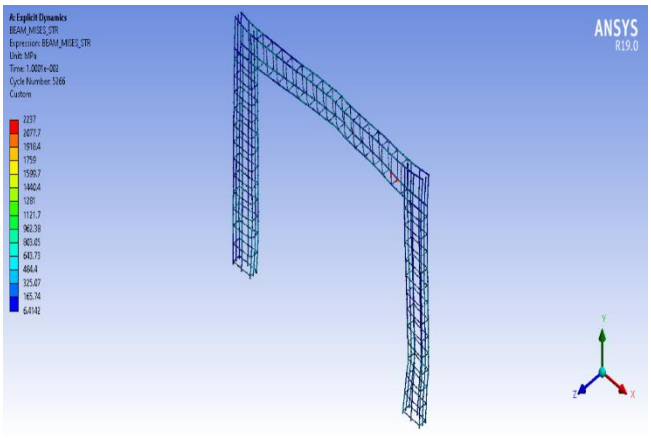

Fig. 13 Equivalent stress rebar for 5m, 100kg

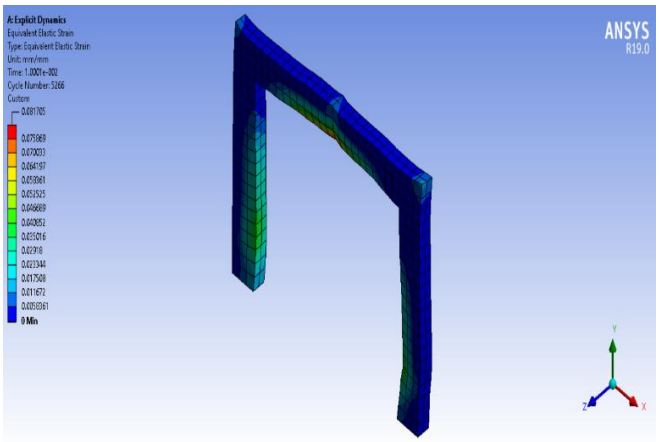

Fig. 12 Equivalent strain for 5m, 100kg

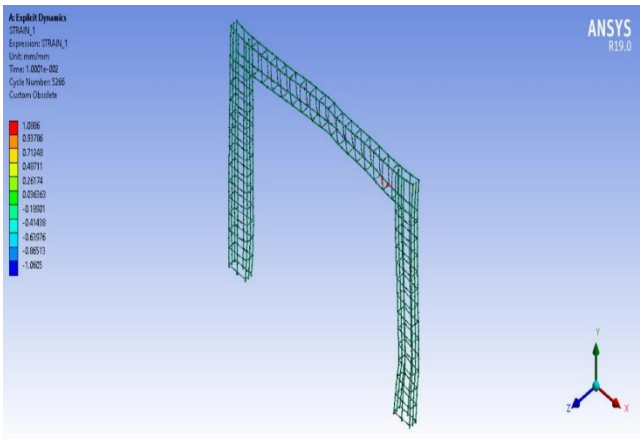

Fig. 14 Equivalent strain REBAR for 5m, 100kg

5.2. Consolidated Peak-Response Results

Table 5 Consolidated peak outputs for all blast cases used for Figures 15–24 and Limit-State tag (LS0–LS4).

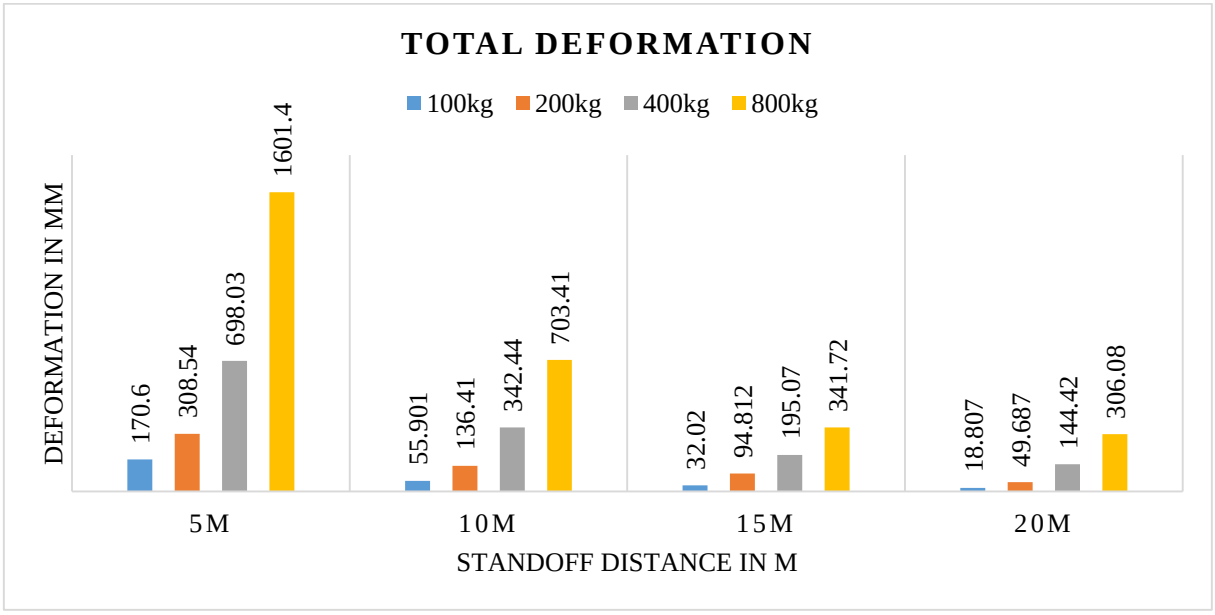

Fig. 15 Total Deformation for 0˚ angle of incidence

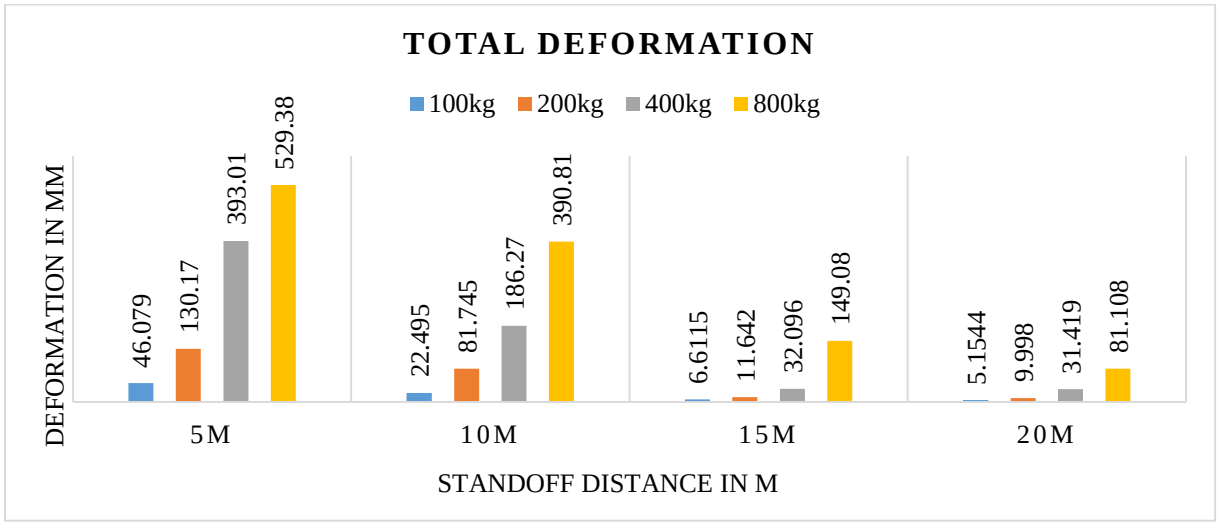

Fig. 16 Total Deformation for 90° angle of incidence

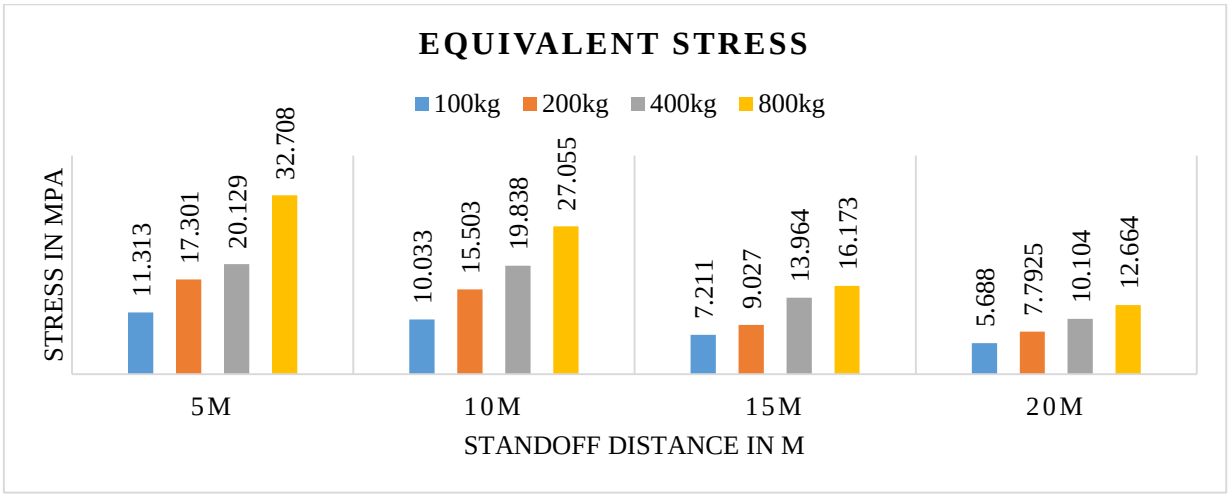

Fig. 17 Equivalent stress of concrete for 0° angle of incidence

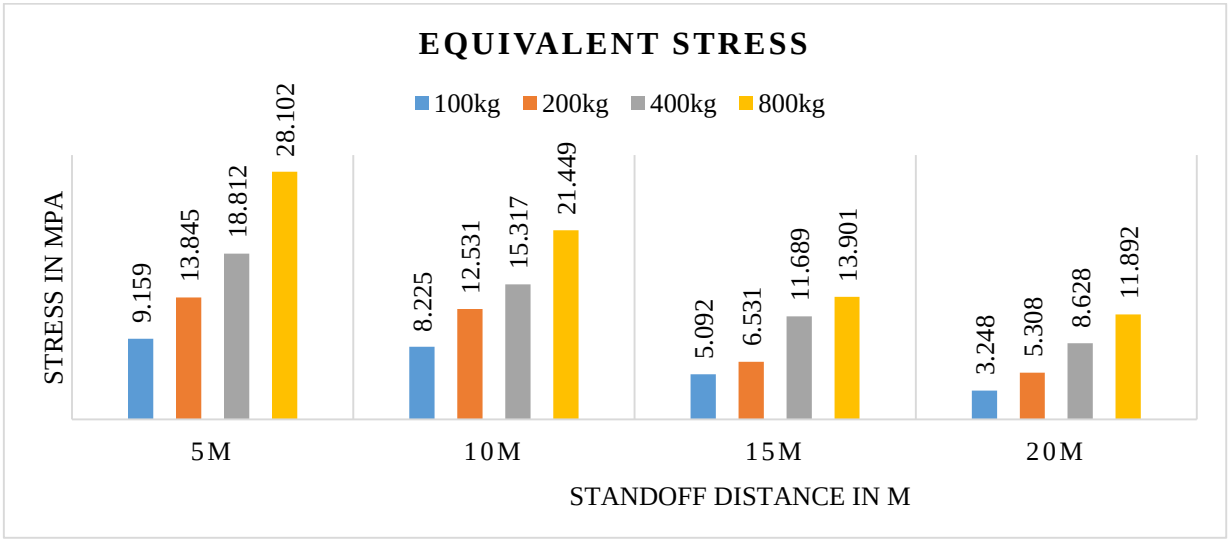

Fig. 18 Equivalent stress of concrete for 90° angle of incidence

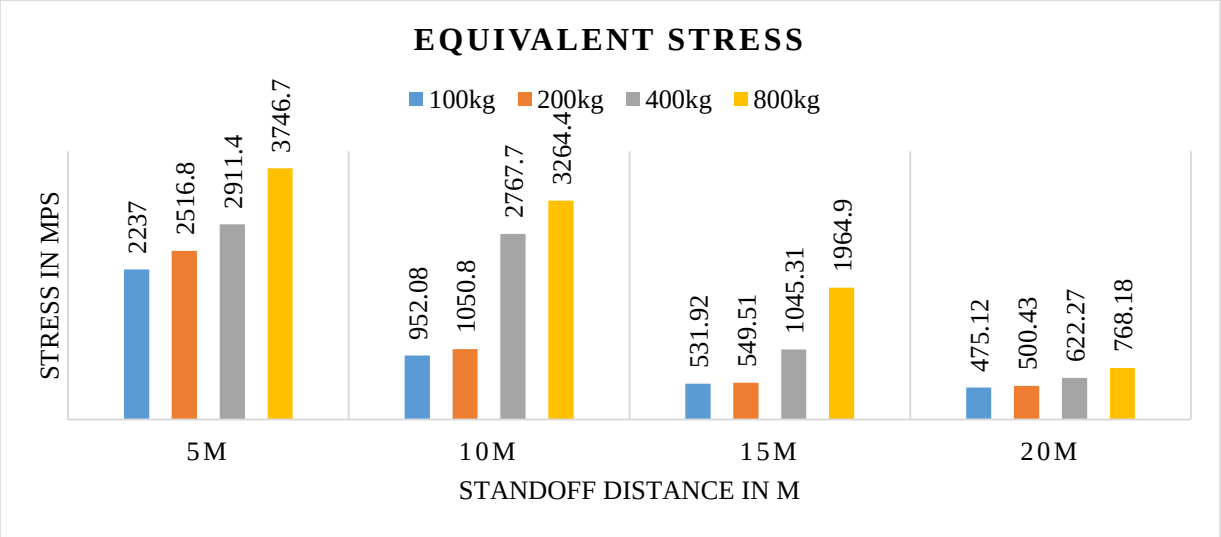

Fig. 19 Equivalent stress of rebar for 0° angle of incidence

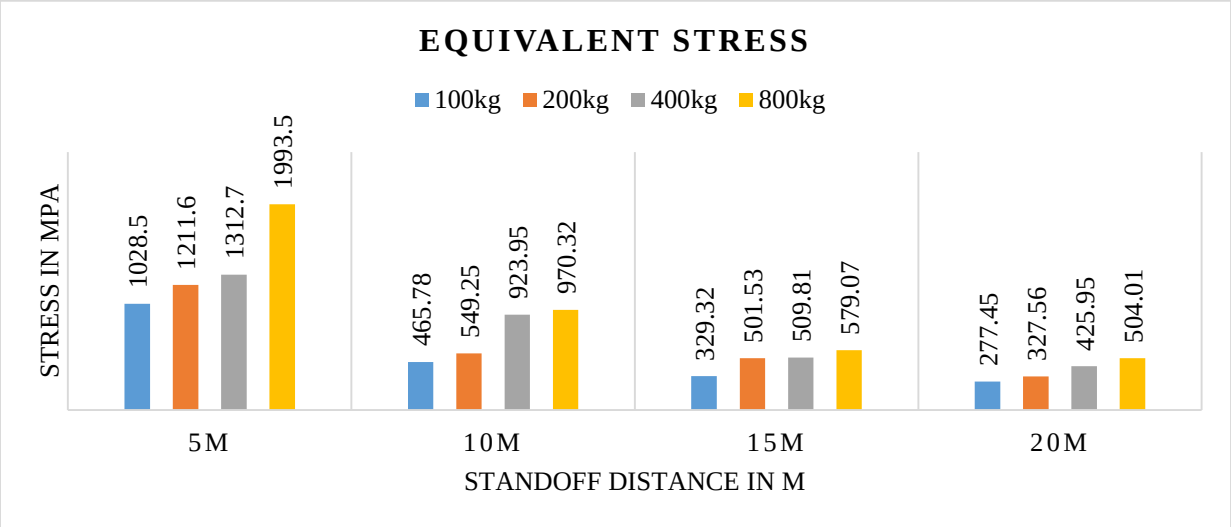

Fig. 20 Equivalent stress of rebar for 90° angle of incidence

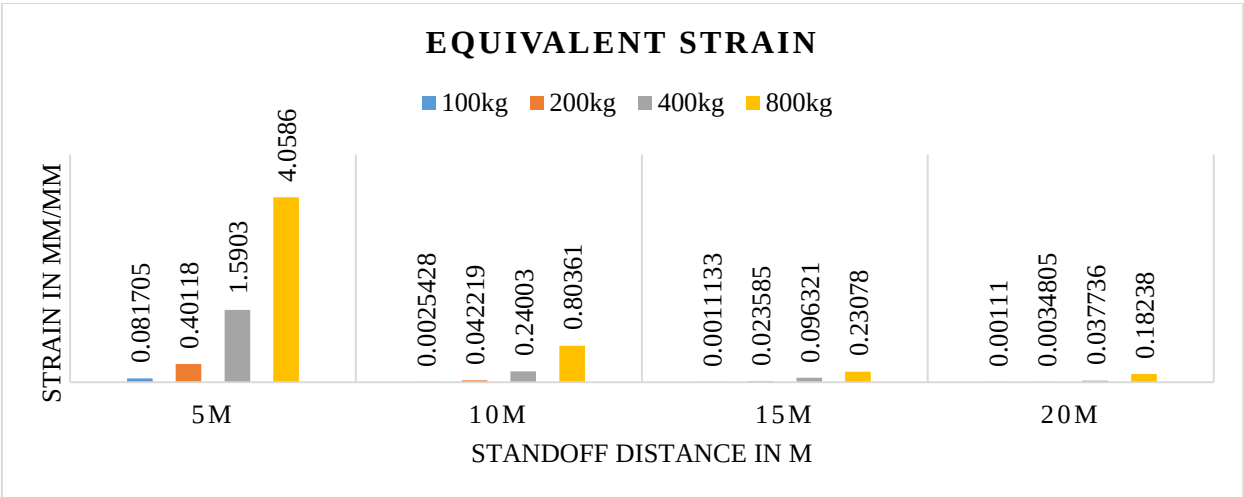

Fig. 21 Equivalent strain of concrete for 0° angle of incidence

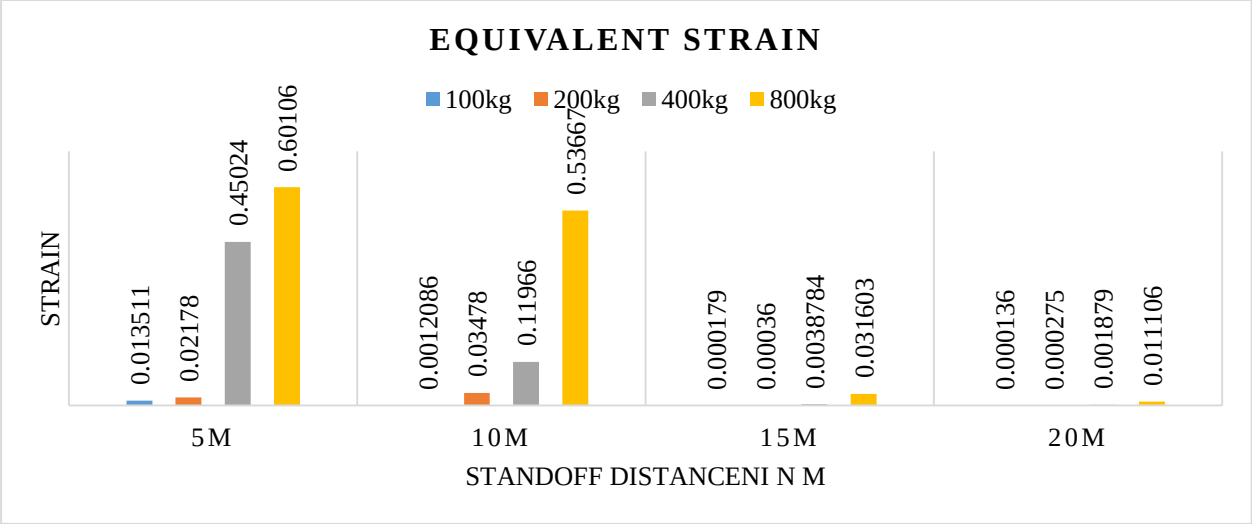

Fig. 22 Equivalent strain of concrete for 90˚ angle of incidence

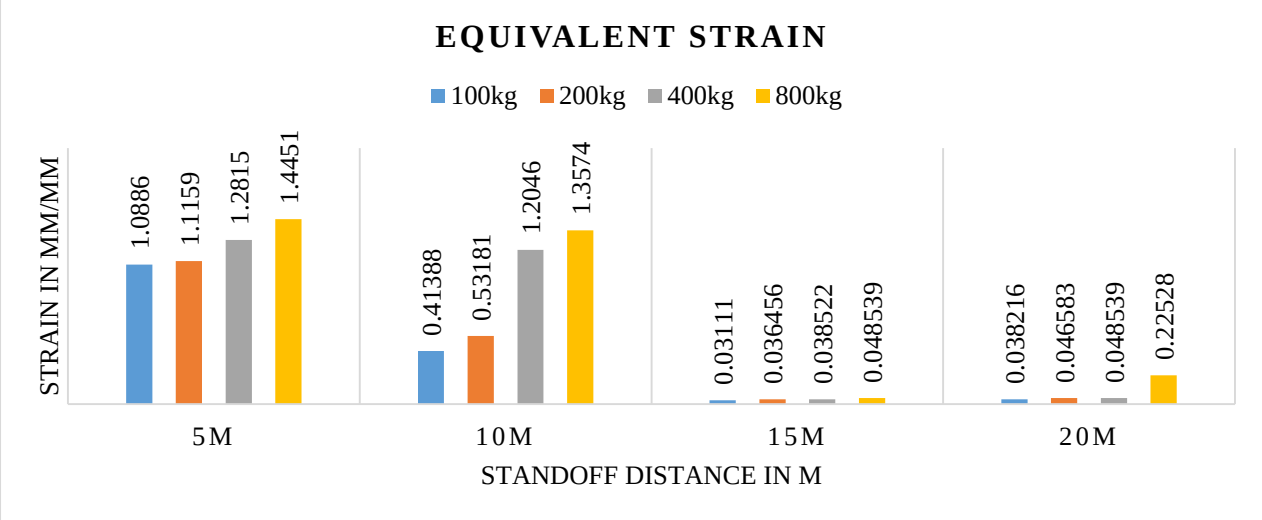

Fig. 23 Equivalent strain of rebar for 0˚ angle of incidence

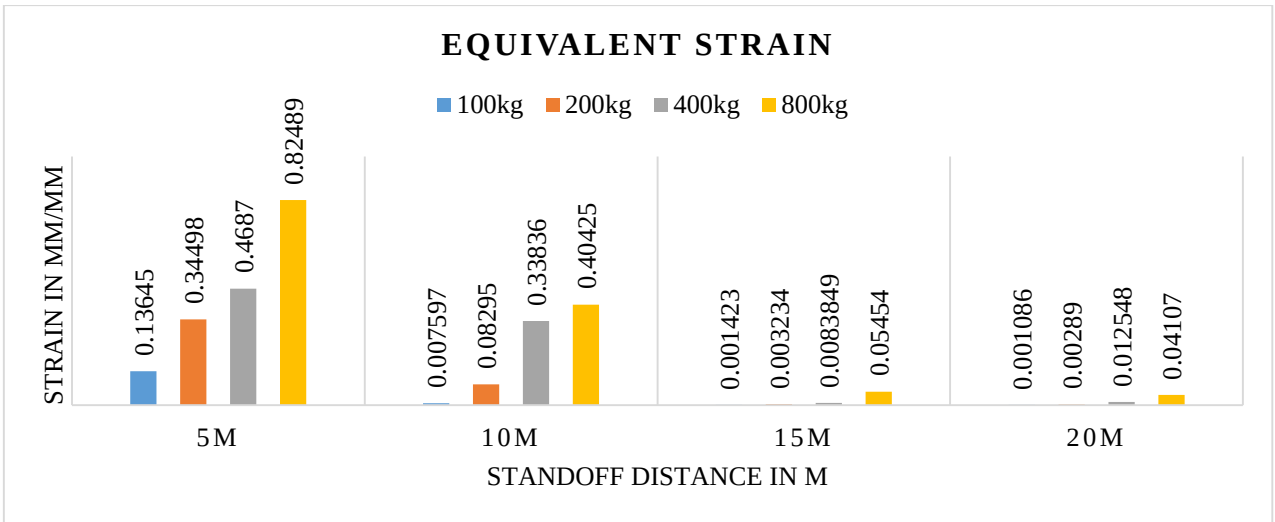

Fig. 24 Equivalent strain of rebar for 90˚ angle of incidence

Table 5. Blast-loading parametric results (θ, R, W): Umax, σeq/εeq in concrete & steel, and LS classification

θ (°)	R (m)	W (kg)	U_{max}	$\sigma_{eq,c}$	$\varepsilon_{eq,c}$	$\sigma_{eq,s}$	$\varepsilon_{eq,s}$	LS
0	5	100	170.6	11.31	0.081	2237	1.088	LS3
0	5	200	308.54	13.84	0.401	2516.8	1.115	LS4
0	5	400	698.03	18.81	1.590	2911.4	1.281	LS4
0	5	800	1601.4	32.70	4.058	3746.7	1.445	LS4
0	10	100	55.901	10.03	0.002	952.08	0.413	LS3
0	10	200	136.41	15.50	0.042	1050.8	0.531	LS4
0	10	400	342.44	19.83	0.240	2767.7	1.204	LS4
0	10	800	703.41	27.05	0.803	3264.4	1.357	LS4
0	15	100	32.02	7.21	0.001	531.92	0.031	LS2
0	15	200	94.812	9.02	0.023	549.51	0.036	LS3
0	15	400	195.07	13.96	0.096	1045.31	0.038	LS3
0	15	800	341.72	16.17	0.230	1964.9	0.048	LS3
0	20	100	18.807	5.688	0.00111	475.12	0.038216	LS2
0	20	200	49.687	7.792	0.003481	500.43	0.046583	LS2
0	20	400	144.42	10.104	0.037736	622.27	0.048539	LS3
0	20	800	306.08	12.664	0.18238	768.18	0.22528	LS4
90	5	100	46.079	9.159	0.013511	1028.5	0.13645	LS2
90	5	200	130.17	13.845	0.02178	1211.6	0.34498	LS3
90	5	400	393.01	18.812	0.45024	1312.7	0.4687	LS3
90	5	800	529.38	28.102	0.60106	1993.5	0.82489	LS4
90	10	100	22.495	8.225	0.001209	465.78	0.007597	LS1
90	10	200	81.745	12.531	0.03478	549.25	0.08295	LS3
90	10	400	186.27	15.317	0.11966	923.95	0.33836	LS3
90	10	800	390.81	21.449	0.53667	970.32	0.40425	LS4
90	15	100	6.6115	5.092	0.000179	329.32	0.001423	LS0
90	15	200	11.642	6.531	0.00036	501.53	0.003234	LS1
90	15	400	32.096	11.689	0.003878	509.81	0.008385	LS2
90	15	800	149.08	13.901	0.031603	579.07	0.05454	LS3
90	20	100	5.1544	3.248	0.000136	277.45	0.001086	LS0
90	20	200	9.998	6.531	0.000275	427.56	0.00289	LS0
90	20	400	31.419	8.628	0.001879	505.95	0.012548	LS1
90	20	800	81.108	11.892	0.011106	564.01	0.04107	LS2

5.3. Parametric Study

5.3.1. Effects of Charge Weight

For fixed stand-off distance and incidence angle, all peak response indicators show monotonic increases with charge weight, reflecting the effects of increased impulse transfer and non-linear structural interaction depth. For normal incidence (θ=0) at R=5 m, U_{max} increases from 170.6 mm for 100 kg to 1601.4 mm for 800 kg, or a factor of 838.69%, which is also the percentage increase over that range of charge weights for deformation demand for the frame. At R=10 m and θ=90 degrees, U_{max} increases from 22.495 mm to 390.81 mm for that same range of charges, yielding an even greater percentage increase (1637.32%). Such changes confirm that charge weight is the principal parameter controlling blast loading intensity, since it governs global deformation demand and non-linear action volume engaged in the structure.

5.3.2. Effects of Stand-Off Distance

Stand-off distance severely reduces structural response with distance due to scaled-distance attenuation of peak overpressure and impulse. For the maximum loading condition (W=800 kg), U_{max} falls by 80.89% with increasing stand-off distance from 5 to 20 m at θ=0, and by 84.68% for θ=90. For all frame loading conditions, maximum deformation demand falls between 79% and 92% with increasing stand-off distance. Such uniform reductions render stand-off distance the most effective geometric parameter for reducing blast loading, since a large overall reduction in structural response is made possible even for frames suffering from high blast loading.

5.3.3. Effects of Incidence Angle

General reductions in peak structural demand occur with varying incidence angle of blast loading for all matched (R, W) pairs. Relative to normal incidence (θ=0) effects (averaged across all cases), U_{max} falls by 65.16%, concrete equivalent stress by 17.56%, concrete equivalent strain by 76.36%, steel equivalent stress by 44.58%, and steel equivalent strain by 74.18% as the incidence angle increases from 0 to 90 degrees, as shown in Table 5. As a result of the effect of incidence angle, its effect on loading patterns can thus be interpreted as localizing the pattern of frame response rather than a generally distributed pattern, as projected loading onto the frame is encouraged to transition from a generally flexural to a more distributed pattern as incidence angle increases.

5.4. LS0–LS4 Limit-State Classifications

A 5-level limit-state classification scheme is defined in terms of solver output parameters to allow for performance-based interpretation of the solver outputs. Using maximum deformation and equivalent strain measures in concrete and steel as output parameters:

Minor damage (LS0) is defined by $U_{max} \leq 10$mm, concrete equivalent strain $\varepsilon_{eq,c} \leq 0.001$, and steel equivalent strain $\varepsilon_{eq,s} \leq 0.005$. Low-repair demand (LS1) corresponds to $10 < U_{max} \leq 50$mm, $0.001 < \varepsilon_{eq,c} \leq 0.01$, or $0.005 < \varepsilon_{eq,s} \leq 0.05$. Moderate, repairable damage (LS2) is characterized by $50 < U_{max} \leq 200$mm, $0.01 < \varepsilon_{eq,c} \leq 0.1$, or $0.05 < \varepsilon_{eq,s} \leq 0.2$. Severe component demand (LS3) is defined by $200 < U_{max} \leq 500$mm, $0.1 < \varepsilon_{eq,c} \leq 0.5$, or $0.2 < \varepsilon_{eq,s} \leq 0.5$. Very severe damage (LS4) corresponds to $U_{max} > 500$mm, $\varepsilon_{eq,c} > 0.5$, or $\varepsilon_{eq,s} > 0.5$.

Application of this framework reveals that the most critical response states cluster at short stand-off distances combined with high charge weights, particularly for ($R = 5$ m, $W \geq 200$ kg)under normal incidence and ($R = 5$ m, $W = 800$ kg) under oblique incidence. Conversely, performance state LS0–LS1 occurs only at higher stand-off distances and lower charge weights, especially under oblique incidence.

5.5. Response Mechanism

The effect of blast angle is much stronger for reinforcement than for concrete, with mean stress reductions of 44.58% for steel and only 17.56% for concrete. Mechanistically, reinforcement demand is mainly determined by the global frame moment/curvature action and tension demand, whose effective broadside projection is reduced by oblique incidence angles.

Concrete equivalent stress, however, is an emergent property of a complex multiaxial stress state involving wave reflections, joint confinement, local effects of the blast loading on column faces, and beam/column interactions. These localized mechanisms are less impacted by a change in the dominant global response mode than the load-bearing demand related to that mechanism, which accounts for the lower magnitude of stress reduction for concrete.

Generalized strains are more affected by incidence angle than stresses, likely because the former is more vulnerable to damage-related inelastic mechanisms such as the opening-closing damage cycles associated with cracks, localization of plasticity, and degradation of stiffness.

Incidence angle mainly suppresses damage-related effects, particularly those related to localized cracking and its localized strain effects, rather than the concentrated stresses that give rise to them. This indicates an indirect intent in the design decision to use incidence angle for resilience improvement: enhancement of resilience via improved deformation capabilities rather than stress management.

From a design perspective, increased stand-off distance and optimal aspect ratio are viable blast reduction design strategies. However, the idealized boundary conditions, the lack of treatment of non-structural elements, and the empirical pressure–time histories used should be borne in mind for any extrapolation of the results to real structures.

5.6. Practical Implications and Limitations

From a design standpoint, results justify using increased stand-off distance and enhanced structural geometry as the primary blast mitigation strategies. However, caveats about idealized boundary conditions, absence of non-structural components, and empirical pressure–time history should be noted when translating results to real structures.

5.7. Response Mechanism

In comparison to the numerical studies of RC structures subjected to blast loading that represent the current state of the art, the current study does not seek to establish improvements in strength or resistance, but in clarity of response interpretation and parameter sensitivity. Existing studies tend to examine isolated components, individual loading configurations, or heterogeneous indicators of damage, complicating comparison of findings. The current study, in contrast, employs solver-consistent global and equivalent stress–strain measures across a structured parametric matrix, permitting a transparent comparison of response severity between variations in charge weight, stand-off distance, and incidence angle.

The explicit parametric inclusion of blast incidence angle as a governing parameter differentiates the current study from the majority of existing literature, in which normal incidence is assumed. By quantifying the influence of loading direction on deformation- and strain-controlled response mechanisms, the current study enhances the interpretive discussion of the viability of geometric and orientation-specific mitigation measures. The findings, therefore, enhance interpretability and usability for performance-based blast design and assessment, rather than seeking marginal improvements in structural performance.

6. Conclusion

Scope and evidence base: Conclusions are drawn from 32 explicit-dynamics blast simulations covering systematic variations in charge weight, stand-off distance, and incidence angle, with response evaluated in terms of peak deformation and equivalent stress/strain demands in concrete and reinforcement. Stand-off distance is the dominant mitigation lever: Increasing stand-off from 5 m to 20 m results in a ~79–92% reduction in peak deformation for all charge levels and incidence angles tested. For the most severe loading ($\boldsymbol{W = 800}$ kg), deformation decreases by 80.89% at $\boldsymbol{\theta = 0}$°and 84.68% at $\boldsymbol{\theta = 90}$°, confirming stand-off as the most effective geometric control on blast demand.

Charge weight drives strongly non-linear response escalation: Holding stand-off distance constant, increasing charge weight from 100 kg to 800 kg produces a huge non-linear amplification of peak deformation by ~+839% to +2155%, depending on geometry and incidence angle, indicating blast loading produces a rapid transition into the large-deformation and damage-dominated response domain. Peak equivalent stresses in both concrete and reinforcement increase monotonically with charge weight, making explosive yield a reliable severity indicator.

Incidence angle appreciably reduces global deformation and damage-related strains: Rotating the blast axis from $\theta = 0°$ to 90° produces consistent reductions in matched-case peak demands, with means of 65.16% in deformation, 76.36% in concrete equivalent strain, and 74.18% in steel equivalent strain. This indicates that the oblique incidence angle reduces blast effects and subsequently, demand levels, by reducing demands that accrue in frame-level sway/curvature, preserving frame function while also reducing the accumulation of inelastic damage-facilitating strain in the regions where damage is expected to accumulate.

Reinforcement demand is more sensitive to incidence angle than concrete stress: Mean reduction in rebar equivalent stress −44.58% is much greater than the mean reduction in concrete stress mean reduction of −17.56%, indicating that reinforcement demands are primarily governed by frame-level flexural/tensile actions curvature which decreases considerably with decreasing impulse projection whereas concrete stress is better maintained by local joint multiaxial effects concrete compression-related shear interaction, compression-induced stress-wave reflections.

Near-field vs far-field scaling differs in steepness of response to charge weight: At near-field stand-off 5 m, peak deformation increases steeply with charge weight, indicating a heavily non-linear impulse-dominated response function. At far-field stand-off 20 m, the deformation-charge function is much less steep, indicating the normalizing influences of reduced impulse transfer and better frame preservation, disregarding boundary effects on the progression into damage-related non-linear response functions.

Recommendations for blast-protected and high-occupancy buildings:

Maximize stand-off distance to the extent possible; it minimizes peak structure demands most consistently across loading scenarios.

Where stand-off cannot be increased, apply blast-informed abnormal load policies, robustness detailing, and progressive collapse resistance; the transition from localized damage to collapse is strongly governed by demands and realistic load-path/boundary-condition effects.

Data Availability Statement

The datasets generated during and/or analyzed during the current study are available from the corresponding author upon reasonable request. Where no new data was created, or where data is unavailable due to privacy or ethical restrictions, a statement is still required.

References

[1] Solomon Abebe, and Tesfaye Alemu Mohammed, "Performance Assessment of Reinforced Concrete Frame under Close-In Blast Loading," *Advances in Civil Engineering*, vol. 2022, no. 1, pp. 1-24, 2022. [CrossRef] [Google Scholar] [Publisher Link]

[2] JiaXin Li et al., "Quantifying Blast Damage and Failure Mode Transition in Reinforced Concrete Columns with a Dimensionless Model," *Scientific Reports*, vol. 15, no. 1, pp. 1-15, 2025. [CrossRef] [Google Scholar] [Publisher Link]

[3] Eslam Abd-El-Nabi, Arafa El-Helloty, and Aymen Summra, "Numerical Analysis of Reinforced Concrete Buildings Subjected to Blast Load," *Structural Concrete: Journal of the Fib*, vol. 24, no. 3, pp. 3727-3743, 2023. [CrossRef] [Google Scholar] [Publisher Link]

[4] Qinghu Xu et al., "Numerical Simulation Study of Progressive Collapse of Reinforced Concrete Frames with Masonry Infill Walls Under Blast Loading," *Modelling and Simulation in Engineering*, vol. 2022, no. 1, pp. 1-16, 2022. [CrossRef] [Google Scholar] [Publisher Link]

[5] Leena Kashiwar, Bajrang Ambhore, and Gaurav Hingwe, "Prediction of Blast Loading and its Impact on Buildings," *International Journal for Research in Applied Science and Engineering Technology*, vol. 13, no. 5, pp. 3309-3319, 2025. [CrossRef] [Google Scholar] [Publisher Link]

[6] Mohamed Ben Rhouma et al., "Damage Assessment of Laboratory-Scale Reinforced Concrete Columns Under Localized Blast Loading," *Buildings*, vol. 15, no. 7, pp. 1-25, 2025. [CrossRef] [Google Scholar] [Publisher Link]

[7] Kartikeya Tiwari et al., "Blast Analysis of Standalone CFST Column," *Materials Research Proceedings*, vol. 49, pp. 396-405, 2025. [CrossRef] [Google Scholar] [Publisher Link]

[8] Wael Ahmed Hemeid, Osama Mahmoud Ali, and Eehab Badr El-deen Khalil, "Non-Linear Behavior of Turbine-Generators Supporting Structure Under Blast Load using Finite Element Analysis," *Aswan University Journal of Sciences and Technology*, vol. 3, no. 1, pp. 164-173, 2023. [CrossRef] [Google Scholar] [Publisher Link]

[9] Sihao Shen et al., "Effect of Charge Eccentric Position on the Response of Reinforced Concrete Columns Under Blast Loading," *Buildings*, vol. 15, no. 11, pp. 1-27, 2025. [CrossRef] [Google Scholar] [Publisher Link]

[10] Hrvoje Draganić et al., "Numerical Investigations of Reinforced Concrete Slabs Subjected to Contact Explosions," *Buildings*, vol. 15, no. 7, pp. 1-21, 2025. [CrossRef] [Google Scholar] [Publisher Link]

[11] Mayuresh Suresh Nalawade et al., "Analysis of Steel Fiber Reinforced Concrete Wall-Column Connection using Headed Bars Subjected to Blast Loading," *World Journal of Advanced Engineering Technology and Sciences*, vol. 17, no. 2, pp. 221-228, 2025. [CrossRef] [Publisher Link]

[12] Ren Jiang et al., "Numerical Investigation on Degradation Mechanism of Reinforced Concrete Structures Under Close-In Explosion," *Advances in Structural Engineering*, vol. 28, no. 9, pp. 1610-1626, 2025. [CrossRef] [Google Scholar] [Publisher Link]

[13] Wensu Chen, Hong Hao, and Shuyang Chen, "Numerical Analysis of Prestressed Reinforced Concrete Beam Subjected to Blast Loading," *Materials and Design (1980-2015)*, vol. 65, pp. 662-674, 2015. [CrossRef] [Google Scholar] [Publisher Link]

[14] Safa Peyman, and Ali Eskandari, "Analytical and Numerical Study of Concrete Slabs Reinforced by Steel Rebars and Perforated Steel Plates Under Blast Loading," *Results in Engineering*, vol. 19, pp. 1-13, 2023. [CrossRef] [Google Scholar] [Publisher Link]

[15] Jun Wu et al., "Numerical Simulation of Reinforced Concrete Slab Subjected to Blast Loading and the Structural Damage Assessment," *Engineering Failure Analysis*, vol. 118, 2020. [CrossRef] [Google Scholar] [Publisher Link]

[16] Jiaxin Li et al., "Analysis of Damage Factors of Reinforced Concrete Frame Under Internal Explosion," *Buildings*, vol. 14, no. 12, pp. 1-20, 2024. [CrossRef] [Google Scholar] [Publisher Link]

[17] Ali Abdelrahim Mohamed, Osama Ali, and Ibrahim M. Metwally, "Blast Performance of RC Columns with Different Levels of Concrete Grades and Reinforcing Ratios," *Structural Concrete: Journal of the Fib*, vol. 26, no. 3, pp. 3282-3304, 2025. [CrossRef] [Google Scholar] [Publisher Link]

[18] Lina M. López et al., "Experimental Response and Numerical Modelling of a Full-Scale Two-Span Concrete Slab Frame Subjected to Blast Load," *Engineering Structures*, vol. 296, 2023. [CrossRef] [Google Scholar] [Publisher Link]

[19] Anton Polyakov, and Oleksandr Lapenko, "Numerical Studies of the Dynamic Impact of the Blast Wave on Protective Structures," *Theory and Practice of Design*, no. 36, pp. 103-115, 2025. [CrossRef] [Google Scholar] [Publisher Link]

[20] Nancy Younan Nasry et al., "Numerical Study for a Reinforced Concrete Structure Under Partially Vented Blast Loads using LS-DYNA and CONWEP Method," *Engineering Research Journal (Shoubra)*, vol. 54, no. 1, pp. 111-119, 2025. [CrossRef] [Google Scholar] [Publisher Link]

[21] Masoud Abedini et al., "Large Deflection Behavior Effect in Reinforced Concrete Columns Exposed to Extreme Dynamic Loads," *Frontiers of Structural and Civil Engineering*, vol. 14, no. 2, pp. 532-553, 2020. [CrossRef] [Google Scholar] [Publisher Link]

[22] Emal Ahmadi, Mehtab Alam, and S.M. Anas, "Blast Performance of RCC Slab and Influence of its Design Parameters," *Resilient Infrastructure: Select Proceedings of VCDRR*, pp. 389-402, 2021. [CrossRef] [Google Scholar] [Publisher Link]

[23] Alok Dua, and Abass Braimah, "Assessment of Reinforced Concrete Slab Response to Contact Explosion Effects," *Journal of Performance of Constructed Facilities*, vol. 34, no. 4, 2020. [CrossRef] [Google Scholar] [Publisher Link]

[24] Evrim Oyguc et al., "Improving Seismic Performance of RC Structures with Innovative TnT BRBs: A Shake Table and Finite Element Investigation," *Applied Sciences*, vol. 15, no. 7, pp. 1-25, 2025. [CrossRef] [Google Scholar] [Publisher Link]

[25] S.M. Anas, Md. I. Ansari, and Mehtab Alam, "Performance of Masonry Heritage Building Under Air-Blast Pressure without and with Ground Shock," *Australian Journal of Structural Engineering*, vol. 21, no. 4, pp. 329-344, 2020. [CrossRef] [Google Scholar] [Publisher Link]

[26] Shangwei Dong et al., *Research on the Conversion Relationship of Nuclear-TNT Blast Loading based on a Protective Door Test Under TNT Blast Loading*, Advances in Frontier Research on Engineering Structures II, Springer, Singapore, pp. 89-102, 2024. [CrossRef] [Google Scholar] [Publisher Link]

[27] Barış Sevim, and Ahmet Tuğrul Toy, "Blasting Response of a Two-Storey RC Building Under Different Charge Weight of TNT Explosives," *Iranian Journal of Science and Technology, Transactions of Civil Engineering*, vol. 44, no. 2, pp. 565-577, 2019. [CrossRef] [Google Scholar] [Publisher Link]

[28] Jihui Geng, and Kelly Thomas, "Dependence of Blast Shielding on Stand-Off Distance," *American Society of Mechanical Engineers 2024 Pressure Vessels & Piping Conference*, Bellevue, Washington, USA, vol. 88490, 2024. [CrossRef] [Google Scholar] [Publisher Link]

[29] Rasid Ahmed Yildiz, "Influence of Stand-off Distance on the Blast-Resistance of Steel Plate Supported Concrete Walls," *International Conference on Applied Engineering and Natural Sciences ICAENS: 5th International Conference on Applied Engineering and Natural Sciences*, Konya, Turkey, vol. 1, no. 1, pp. 232-237, 2023. [CrossRef] [Google Scholar] [Publisher Link]